GIF Irradiation Test with an 8-Plane TRT Endcap Sector Prototype

Anatoli Romaniouk, Juan Valls
CERN

Abstract

In this document we report the results from a a study of the performance under high rates of an endcap TRT 8-plane sector prototype placed in the Gamma Irradiation Facility (GIF) at CERN. This represents a total 192 fully instrumented straws with close to final electronics. After describing the electrical characterization of the front-end electronics, results will be presented in terms of occupancies and noise rates under irradiation. We study also possible sources of cross-talk and common mode noise between straws which affect the overall performance of the system.

1) The Gamma Irradiation Facility

The Gamma Irradiation Facility (GIF) [1] is a test area placed at the West Area of the CERN SPS where high energy particle detectors are exposed to a particle beam in the presence of a high background flux of photons. These conditions are used to simulate the operation of the detectors at the Large Hadron Collider. The GIF is situated at the downstream end of the X5 test beam (see Figure 1).

The GIF provides 662 keV photons produced by a strong radioactive ^{137}Cs source (740 Gbq) which permits to irradiate detectors of up to 6 by 6 m^2 area at 5 meters distance from the source. At 4 meters distance from the source the flux is ~10^5 photons/cm^2/s, with a maximum photon flux of ~10^7 photons/cm^2/s at 1 m where the TRT sector prototype was placed.

The TRT sector prototype is surrounded by a ~1 mm Aluminum converter, which leads to a straw hit probability per photon of ~0.5-1.0%. This leads to a charged particle rate on the straws of ~5×10^4 electrons/cm^2/s, still below the expected levels at the LHC (~10^6 particles/cm^2/s).

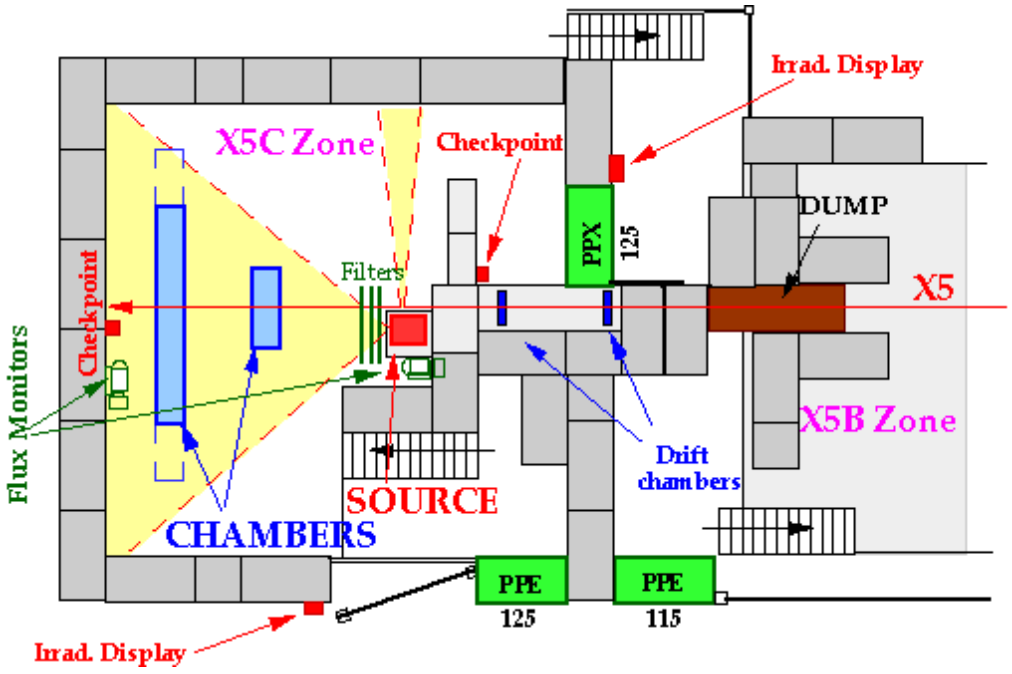

Figure 1: Layout of the Gamma Irradiation Facility (GIF) at CERN.

2) Experimental Setup

The experimental setup consists of a TRT sector prototype of an endcap wheel of type A (1/32 of φ) used for test beam measurements (Figure 2). The sector prototype contains 8 planes of 24 instrumented straws (192 total straws). Each straw is 39 cm long with a 4 mm diameter. The construction of the detector followed the TRT rules and guidelines for grounding and shielding.

In the sector prototype two arc-shaped printed circuit boards (web boards) bring the signals from the straws to the connectors at the top (outer radius) where the front-end boards are connected.

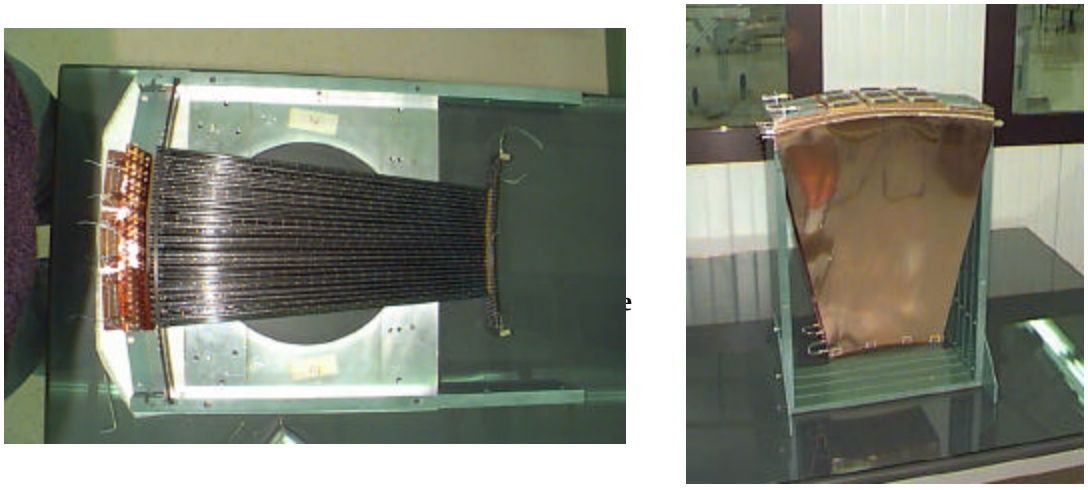

Figure 2: 8-plane TRT endcap sector prototype.

The TRT front-end endcap boards consist of 3 printed circuit boards connected between them with two kapton strips (flex-rigid board, Figure 3). Each printed circuit board groups 4 DTMROC chips (16×4=64 channels) and is connected to another printed circuit board with 8 ASDBLR chips. Each DTMROC is able to serve 2 ASDBLR chips and 16 straws. Two web boards are used as the electrical interface between the straws and the flex-rigid board.

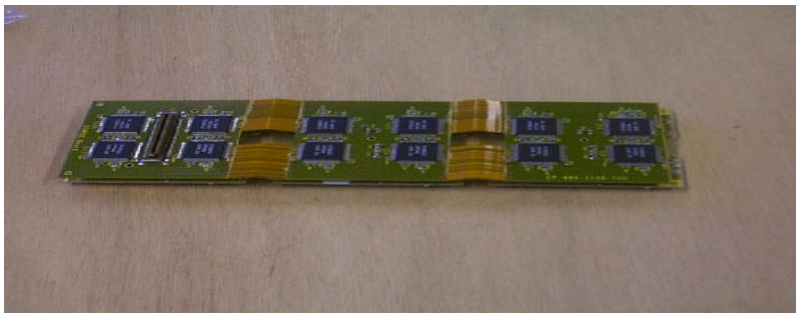

Figure 3: Flex-rigid front-end board with 12 DTMROC and 24 ASDBLR chips (192 channels).

All results reported in this paper have been obtained for the DMILL 99 version of the DTMROC and ASDBLR chips.

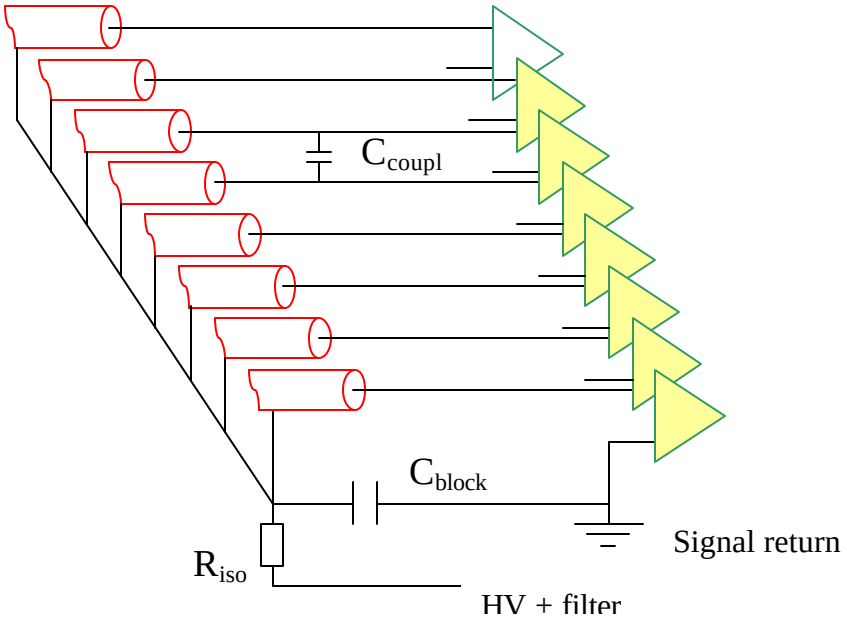

Figure 4: Schematic diagram of the TRT front-end electronics. R_{iso} is the isolating resistor that separates the straw groups from each other at high frequency. C_{block} is the blocking capacitor between a group of 8 straws and the electronics, which carries the high frequency signal return between the straw and the front-end analog chip. C_{coupl} represents the parasitic coupling capacitance.

An individual HV power line serves one single flex-rigid board. Cathode straws are grouped together in sets of 8 to share one HV blocking capacitor, so there are a total of 24 capacitor groups per flex-rigid board. Figure 4 shows a simplified schematic arrangement of TRT HV elements for a HV group. Each capacitor group requires an isolating resistor to separate it from the other groups at high frequency.

The active gas in the straws was a mixture of 70% Xe, 20% CF_4, and 10% CO_2. The sector prototype was operated at a gas flow of 0.08 cm^3/min per straw, which corresponds to about one volume per hour.

2) DAQ and Software: XTRT

The data acquisition and readout system used for the measurements was based on the miniROD VME board (which is a scaled down version of the ROD). A TTC VME board

provides the clock, trigger and other commands both to the front-end electronics and the miniROD. The interface between the front-end electronics and the back-end VME boards is provided by a prototype patch panel. All data was taken with internal TTC random triggers at 40 MHz.

We use the XTRT software [2] developed for system tests for data taking. The XTRT software provides a diagnostic tool for electrical characterization of TRT electronics. It also provides a GUI (Graphic User Interface) to display occupancies and hit multiplicity distributions as online histograms or through a straw event display.

3) Electrical Characterization of Boards

The electrical characterization of the front-end electronics was done in terms of calibration measurements of individual ASDBLR channels, the study of the noise performance and threshold spread.

2.1) Calibrations

Two different sets of calibration measurements were done at the lab:

1. Calibration of individual DTMROC chip DAC's, which provides a relationship between DAC counts and voltage at the discriminator inputs.

2. Calibration of individual ASDBLR channels. These calibrations provide a relationship between an input signal amplitude (either in volts and or in terms of eV energy) and discriminator threshold (in volts or DAC counts).

For the first set of measurements the output DAC voltages from threshold scans on the DTMROC chips of the flex-rigid board were measured with CAMC voltage ADC modules (Le Croy 2232A 32-input differential ADC). Figure 5 shows the distribution of slopes (in V/DAC) for the low threshold DAC's (low0 and low1) and high threshold DAC's (high0 and high1). Table 1 summarizes the average results for the 12 DTMROC chips for the low and high thresholds.

	low0	**low1**	**high0**	**high1**
mV/DAC	5.3 ± 0.2	5.3 ± 0.1	5.3 ± 0.1	5.3 ± 0.5

Table 1: Calibration average results for the low and high thresholds of the 12 DTMROC chips of the flex-rigid board.

For the measurement of the second set of calibrations we performed threshold scans for different input voltages into the ASDBLR chips. Test pulse signals from the TTC were

fed into a NIM dual timer, a set of attenuators, a linear splitter and, finally, into a set of injector boards. These injector boards were designed to mimic the signal shape of point ionizations in a TRT straw filled with a Xenon based fast gas. They have been calibrated to provide 8.5 mV per 4 keV of deposited charge.

S-curves from threshold scans for each input voltage were fit to complementary error functions (Section 2.1). From these fits, the offsets (50% S-points) and slopes for each ASDBLR channel were extracted. Figure 6 shows the typical relation between input signal amplitude (in mV) and discriminator threshold (in DAC counts) for 16 channels of a DTMROC chip (2 ASDBLR chips). Figure 7 shows the distribution of gains (in DAC/mV and DAC/eV) and DAC offsets for all channels of the flex-rigid board used in this work. The corresponding gain values in V/eV and voltage offsets (in mV) are shown in Figure 8. On average we obtain that a 283 mV threshold level corresponds to 200 ± 46 eV energy threshold. All averages are done for channels with a good response to charge injection (179 out of the total 192 channels of the flex-rigid board, see Table 2).

The ASDBLR chips used in these measurements have also been calibrated at Penn University with a different setup. Penn gain results are given in terms of V/fC and voltage offsets in mV. Figure 9 compares Penn calibration results with those obtained at CERN if we assume a 1 fC = 140 eV correspondence. Finally, Figure 10 compares Penn and CERN results for gains and offsets as a function of channel number.

A summary of average gains and offsets over all ASDBLR channels of the flex-rigid board used in this work is tabulated in Tables 3 and 4 for the CERN and Penn measurements, respectively.

ROC Number	Bad Channels	ROC Number	Bad Channels
ROC 0	4	ROC 6	11
ROC 1		ROC 7	
ROC 2	11	ROC 8	
ROC 3	5, 7	ROC 9	8, 9
ROC 4		ROC 10	3, 11, 12
ROC 5	3	ROC 11	3, 11

Table 2: Channels with a bad response to charge injection.

	DAC/mV	DAC/eV	DAC offset
CERN	76.1 ± 8.0	0.16 ± 0.02	24.1 ± 6.6

Table 3: Gain and offset averages over all ASDBLR channels for the CERN measurements (179 working channels out of the total 192 channels).

	mV/eV	mV/fC	V offset (mV)
CERN	0.81 ± 0.08	114 ± 11	121 ± 34
Penn		114 ± 7	133 ± 36

Table 4: Gain and offset averages over all ASDBLR channels for the Penn measurements (192 channels).

2.1) Noise Measurements

We define a S-curve as a probability *P(t)* of surpassing a given threshold t. If we assume an intrinsic noise purely Gaussian and the absence of other noise sources, *P(t)* is given by the complementary error function *Erfc(t):*

$$Erfc(t) = 1 - Erf(t) = 1 - \frac{2}{\sqrt{p}} \int_0^t e^{-t^2} dt$$

The noise can then be measured from threshold scans by fitting each single channel S-curve to a complementary error function. The result of the fit provides the sigma noise (S-curve slope) and offset (50% S-point).

Figure 11 shows the fit results of S-curves taken from threshold scans for each of the 12 DTMROC chips of the flex-rigid board. S-curves are calculated as low threshold occupancies as a function of the low threshold (in DAC counts) with the flex-rigid board connected to the sector prototype straws.

Figure 12 shows the sigma noise distribution of the 192 channels of the flex-rigid board and with the straws connected to the front-end electronics. Results are given both in DAC counts and in eV's (after applying the calibration results obtained in Section 2.1). The average noise for the 192 channels is measured to be 38.0 ± 6.1 eV, which corresponds to 1696 ± 272 electrons for a 1 fC = 140 eV correspondence (12375 ± 381 electrons if we assume 1 fC = 100 eV).

2.2) Threshold Spread

We have also measured the channel-to-channel offset variation on the thresholds for each ASDBLR chip present in the flex-rigid board. Figure 13 shows the offset threshold spread with respect to a nominal 200 eV chip average for 12 out of the 24 ASDBLR chips. The same distribution for the 192 channels of the flex-rigid board is shown in Figure 14. In all cases the spread is always below ± 50 eV.

4) Performance Under Irradiation

The low threshold occupancies, leading edge occupancies, and noise rates, averaged over all working channels connected to the straws, and without irradiation are summarized in Table 5 for a nominal low threshold of 200 eV. Non-working channels are defined either as having a bad response to charge injection (see Table 2), being noisy (occupancies above 5%) or dead. Low threshold occupancies are defined as the ratio of events with at least one bit set. Leading edge occupancies are defined as the ratio of events with at least one leading edge present over the total number of events. Both occupancies and rates are calculated for 3 beam crossings.

	Occupancies (%)	**Rates (kHz)**
Low Threshold	1.1 ± 1.1	143 ± 143
Leading Edge	1.0 ± 1.1	130 ± 143

Table 5: Low threshold and leading edge average noise occupancies and rates averaged over all working channels of the flex-rigid board connected to the straws. All values are given for 3 beam crossings.

Under GIF irradiation, the averaged low and high threshold hit occupancies and noise rates are shown in Figures 15 and 16, respectively, as a function of threshold. All channels are averaged over all working channels of the flex-rigid board, and calculated for 3 beam crossings. Table 6 shows these values for the nominal low threshold of 200 eV and high threshold of 5 keV.

	Occupancies (%)	**Rates (kHz)**
Low Threshold	6.1 ± 2.4	793 ± 312
Leading Edge	5.0 ± 2.1	650 ± 273
High Threshold	1.8 ± 0.4	234 ± 52

Table 6: Low threshold and leading edge average occupancies and rates averaged over all working channels of the flex-rigid board connected to the straws. All values are given for 3 beam crossings.

Figures 17 and 18 show the low and high threshold hit occupancy distributions for a 200 eV low threshold and a 5 keV high threshold, respectively, under GIF irradiation. The low threshold occupancies are given in terms of leading edge occupancies (at least one LE in 3 beam crossings), and low level hit occupancies (at least one low threshold bit set in 3 beam crossings). High threshold hit occupancies are also given for 3 beam crossings.

5) Cross-Talk Occupancies

The low and high threshold occupancy distributions under GIF irradiation (Table 6) are shown in Figure 18 as a function of channel number. Although there is no evident occupancy cross-talk between straws, the most detailed information on the correlation between the signals from different channels is obtained from the occupancy correlation matrix. This correlation matrix (see, for example, reference [3]) is defined as:

$$r_{ij} = \frac{OPC_{ij} - OPC_i OPC_j}{\sqrt{OPC_i - OPC_i^2}\sqrt{OPC_j OPC_j^2}}$$

where OPC_i represents the average occupancy for channel i and OPC_{ij} corresponds to the average occupancy for an hypothetical channel which represents the logical AND of channels i and j. Figure 19 shows the correlation matrix for two different DTMROC chips (16 channels each). A clear cross-talk between channels from two ASDBLR HV groups is visible as two band structures around the diagonal.

5.1) *Sources of Cross-talk*

There are two main sources of cross-talk between the straws. First, straws which share the same decoupling capacitor suffer conductive coupling on their signal return (see Figure 4). Second, although the straw wall surrounds its wire all over the length of the straw, it is still possible an exposure to the environment at the end of the straw (parasitic capacitive coupling). The internal channel-to-channel cross-talk of the analog read-out ASDBLR chip is by design less than 0.5%. Finally, the connecting traces on the web boards which serve the signals from the straws to the front-end electronics may also contribute to the detected straw-to-straw cross-talk.

The effective cross-talk is a superposition of all mentioned coupling paths. Measurements and calculations [4] suggest results in the percentage region, but the final cross-talk can reach a manifold of these results. As 8 straws are connected to a common HV capacitor, one straw will see the cross-talk of the other 7 straws, mainly conductive, when they are fired.

5.1) *Occupancy Cross-talk*

In order to understand the source of the cross-talk seen in Figure 19 we now study the occupancies for three different sets of straws and for events where only one particular straw is required to contain a high threshold hit (at least one high threshold bit set out of

the 3 beam crossings). We will refer to this straw as the *trigger straw*. We consider then the average occupancies for the following set of straws:

- 7 straws sharing the same HV group as the *trigger straw*.
- 24 straws (from 2 DTMROC chips) sharing the same web flap as the *trigger straw* (not included are those straws sharing the same HV group as the *trigger straw*).
- 64 straws from 4 DTMROC chips placed in different web flaps as the *trigger straw*. We will refer to these straws as *away straws.*

In all cases we consider only channels not suspected of bad behavior (dead or noisy channels). The situation is illustrated in Figure 20, where 4 DTMROC chips are shown, including one with the *trigger straw*, one sharing the same web flap as the *trigger straw*, and 2 away DTMROC chips placed on different web flaps as the *trigger straw*.

Figure 21 shows the low threshold occupancies for the above 3 sets of straws. Results are shown as a function of the low threshold and for a 5 keV high threshold on the *trigger straw*. Figure 22 shows the same occupancies but as a function of the high threshold set on the *trigger straw* and for a 200 eV low threshold. All results are under GIF irradiation.

In order to check whether a contribution from physics accounts to for the measured cross-talk we repeat the distributions in Figures 21 and 22 when a high threshold veto is set on the nearby straws to the *trigger straw*. No significant change is observed on the occupancies for the 7 straws sharing the same HV group as the *trigger straw.*

One can also study the distribution of the number of fired straws for the 7 straws sharing the same HV group as the *trigger straw*. This distribution is shown in Figure 23 compared to the case where no hit requirement is set on the *trigger straw*. In nominal conditions (with no hit requirement on the *trigger straw*) the straw multiplicity distribution is peaked at 1. If a high threshold hit is required on the trigger straw and some sort of physics cross-talk would be expected, this distribution would still be peaked at low values. Nevertheless, Figure 23 shows a flat distribution for the straw multiplicity, which suggests the same charge is shared among all the straws.

From Figures 21 and 22 we observe a factor 5 increase (from 5% to ~ 25%) on the low threshold occupancies on straws sharing the same HV group as the *trigger straw* (for a nominal 200 eV low threshold). One can deduce then an upper limit on the amplitude cross-talk of 200 eV/5000 eV = 4%.

If one change the requirements on the trigger straw to contain a leading edge hit (at least one leading edge in 3 beam crossings) instead of a high threshold hit, the occupancies do not change. They decrease, though, if a high threshold veto is required on the nearby straws to the *trigger straw*. Figure 24 shows the low threshold occupancies for the above 3 sets of straws as a function of the low threshold with and without the high threshold veto.

Finally, Figure 25 shows the high threshold occupancies as a function of the high threshold on the *trigger straw*.

5) Conclusions

We have studied the performance of an endcap TRT 8-plane sector prototype under the GIF photon irradiation facility at CERN. This facility provides a total photon flux of ~ 10^5 photons/cm^2/s, which converts to charged particle rates of ~ 5×10^4 electrons/cm^2/s.

A full characterized flex-rigid board with ASDBLR99 and DTMROC99 chips (192 channels) was used for the measurements. At nominal operating conditions (200 eV low threshold and 5 keV high threshold) the observed total occupancies were ~6.1% (low threshold), 5.0% (leading edge), and 1.8% (high threshold) for 3 bunch crossings. This represents low threshold, leading edge, and high threshold rates of ~793 kHz, ~650 kHz, and ~234 kHz, respectively.

We do not observe an increase in the low threshold occupancies from amplitude cross-talk between straws for low threshold signal hits. Nevertheless, high threshold hits seem to increase the low threshold occupancies on nearby straws by factors of up to 5. This occupancy cross-talk is thought to come from conductive capacitive coupling of the HV group arrangment of the TRT front-end electronics. The corresponding amplitude cross-talk calculated from this occupancy cross-talk is estimated to be less than 4%.

The photon flux provided by the GIF facility at CERN is still well below the expected charged particle rates at LHC of ~ 10^6 particles/cm^2/s. The study presented here will be repeated at higher rates at the Weizmann Institute facilities in Israel where a ^{60}Co source of 1.17 MeV and 1.33 MeV photons is available. This will allow to repeat the tests at charged particle rates of ~5×10^6 electrons/cm^2/s, very close to the expected LHC rates.

6) Acknowledgements

The authors thank Philippe Farthouat, Daniel Froidevaux, Peter Lichard, Steven Passmore, and Ole Rohne for all the help received in this work.

References

[1] L. Gatignon, *The West Experimental Area at the CERN SPS*, CERN SL-2000-016 EA.
S. Agosteo et al., *A Facility for the test of large-area muon chambers at high rates*, Nucl. Instr. and Meth. **A 452** (2000) 94.

[2] J. Valls, *XTRT – A Program for TRT System Tests,* document in preparation, http://cern.ch/valls.

[3] L. Feld *et al*., *Measurement of Common Mode Noise in Binary Read-Out Systems,* ATL-INDET-2001-006.

[4] P. Lichard, private communication.
A. Manara *et al*., *Cross-Talk Studies with the Endcap Sector Prototype*, talk presented at the Cracow TRT week, May 1999

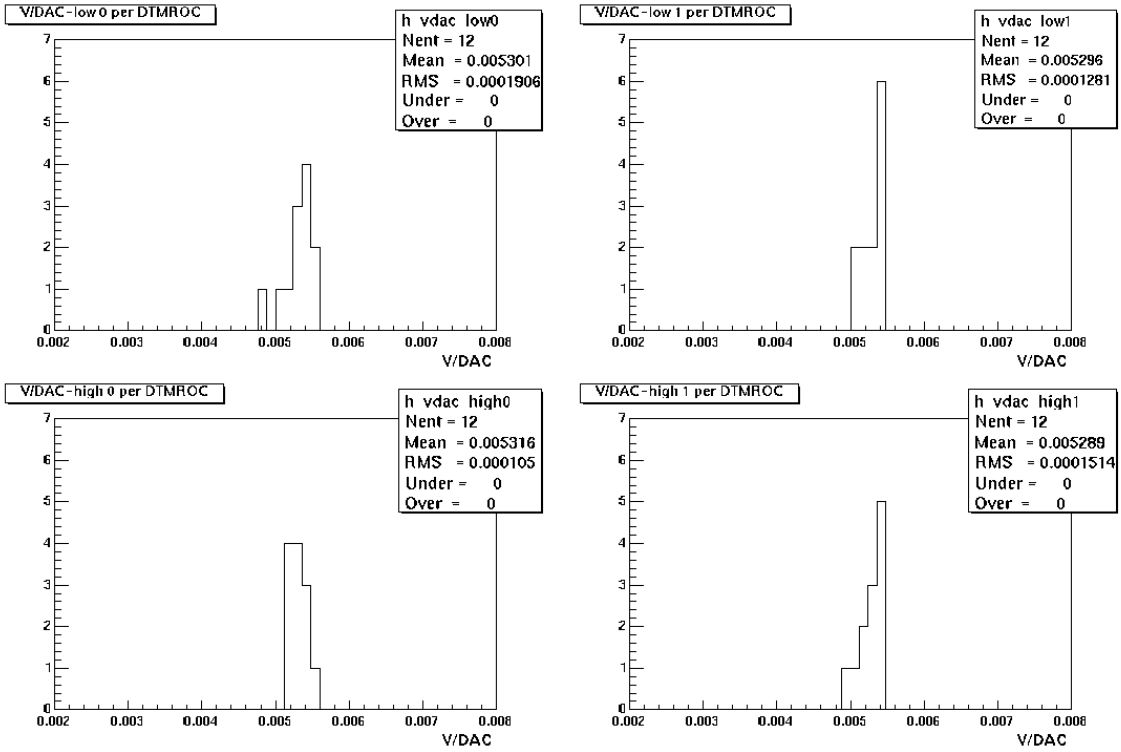

Figure 5: Calibration results for the low0, low1, high0 and high1 DAC thresholds of the 12 DTMROC chips of the flex-rigid board used in this work (all units in V/DAC).

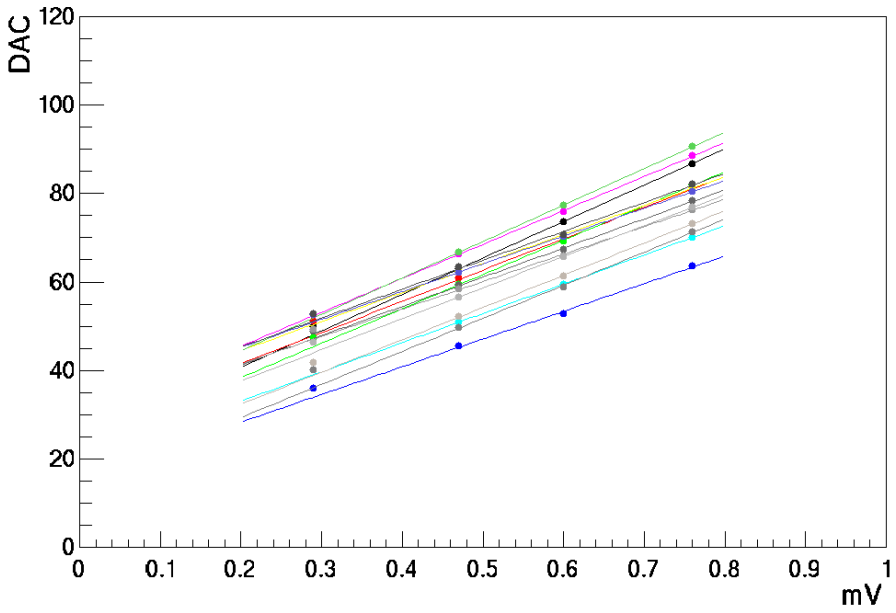

Figure 6: Low threshold (in DAC counts) versus pulseheight (in mV) for 16 channels of a DTMROC chip.

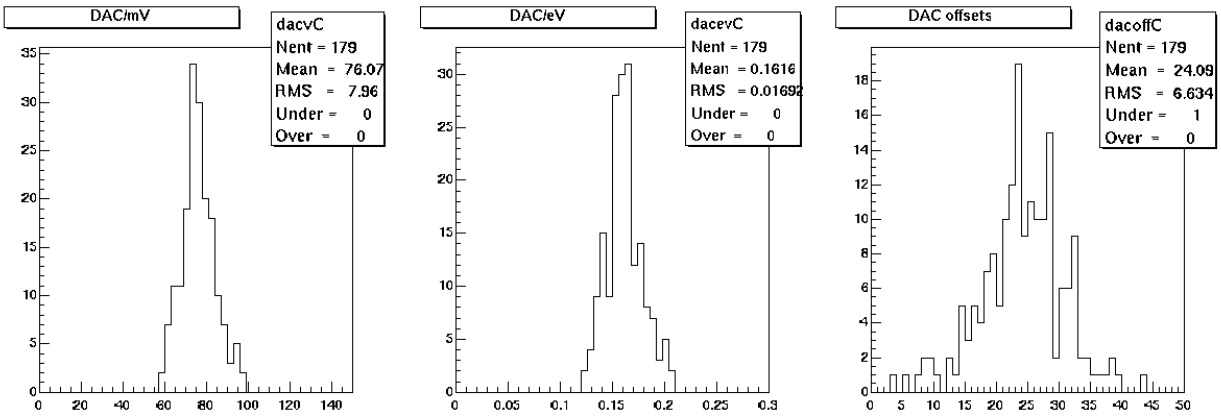

DAC/mV DAC/eV DAC Offsets

Figure 7: Distribution of gains (in DAC/mV and DAC/eV) and DAC offsets for all working channels of the flex-rigid board used in this work.

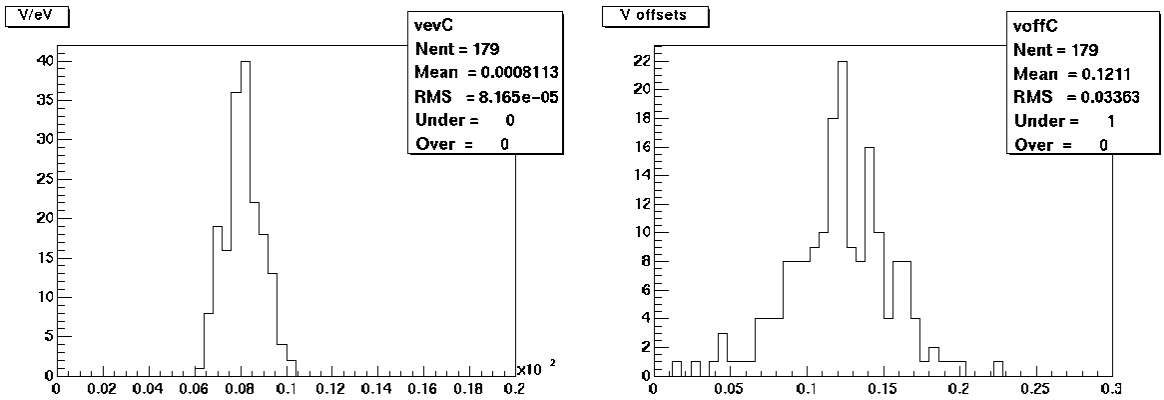

V/eV V Offsets

Figure 8: Distribution of gains (in V/eV) and voltage offsets (in mV) for all working channels of the flex-rigid board used in this work.

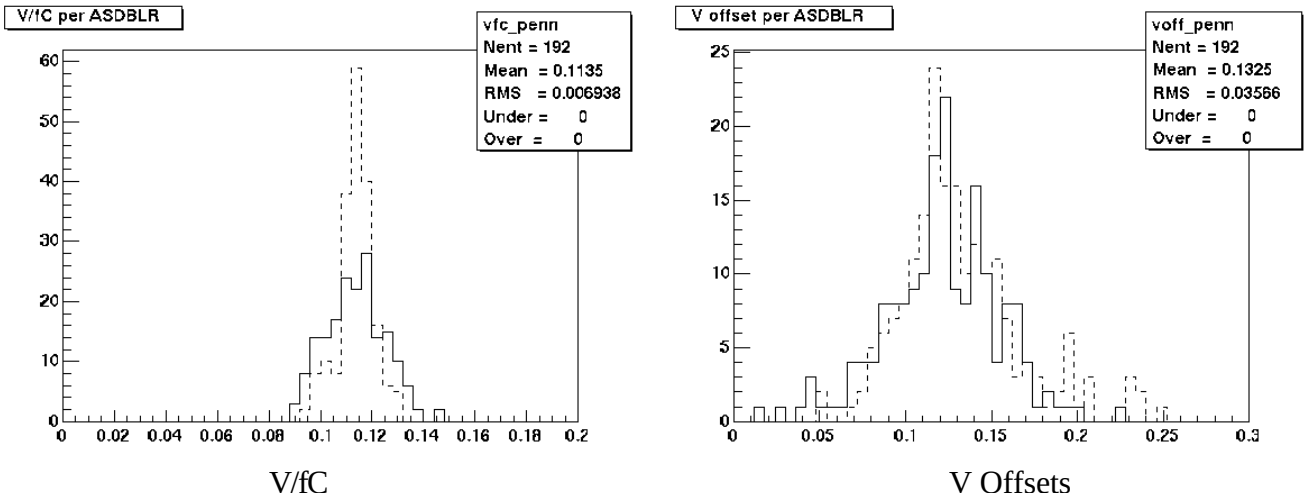

Figure 9: Distribution of gains (in V/fC, right plot) and voltage offsets (in volts, left plot) for all working channels of the flex-rigid board used in these measurements. Solid histograms correspond to the CERN measurements and dashed histograms correspond to Penn measurements.

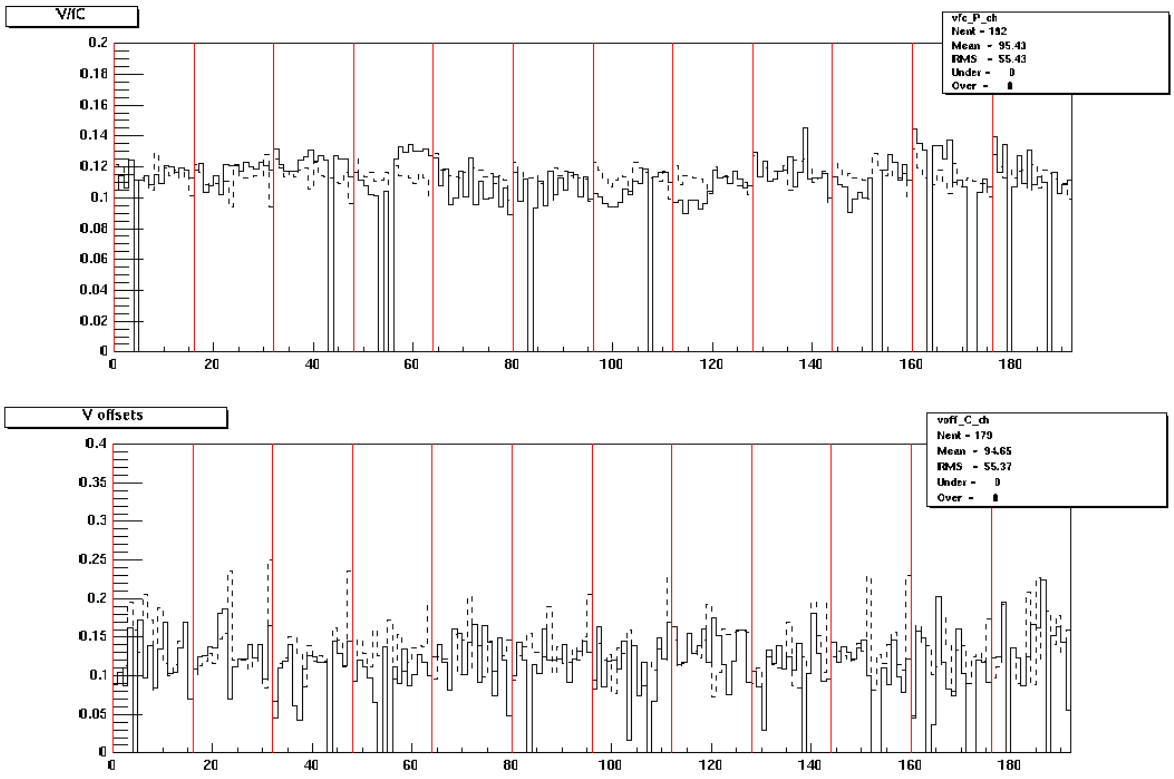

Figure 10: Distribution of gains (in V/fC) and voltage offsets (in volts) as a function of channel number. Solid histograms correspond to the CERN measurements and dashed histograms correspond to Penn measurements.

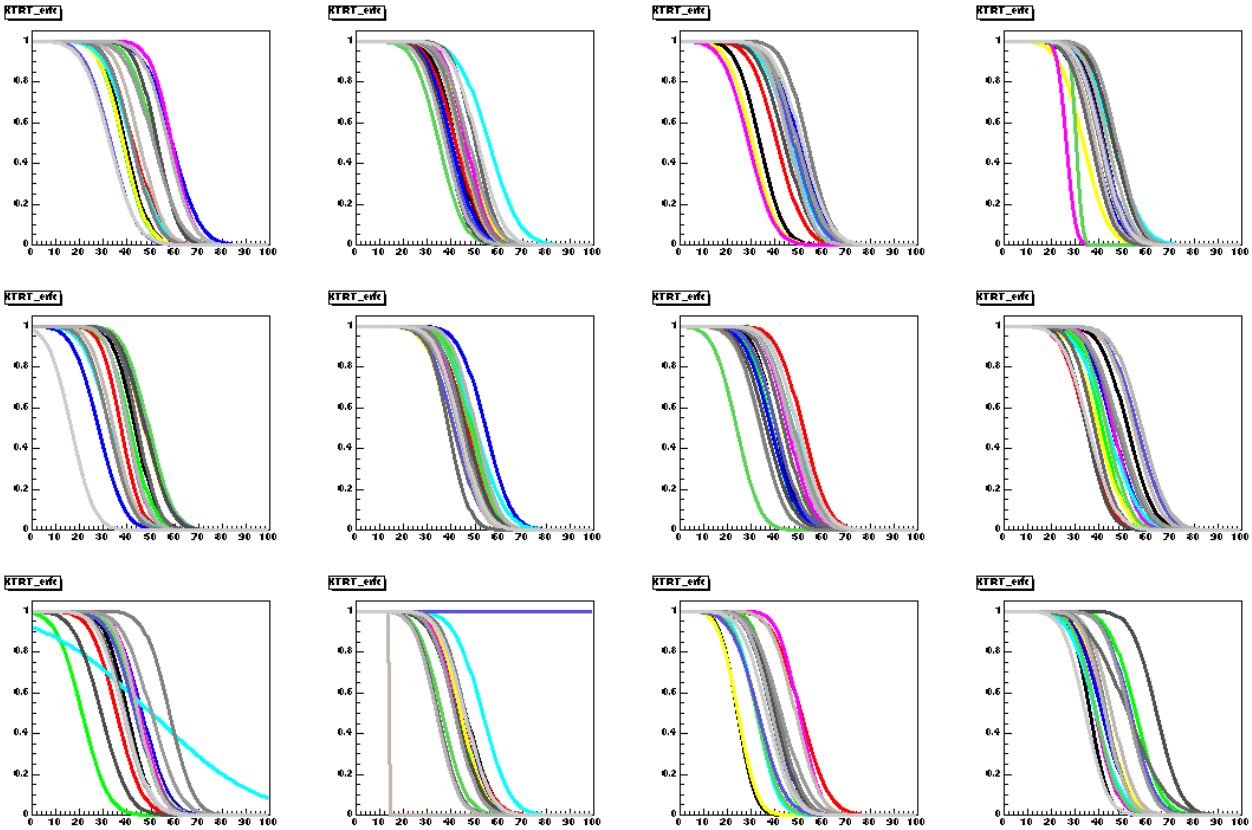

Figure 11: S-curves (low threshold occupancies as a function of the low threshold in DAC counts) for the 12 DTMROC chips of the flex-rigid board. Each plots shows results for 16 channels. All curves are obtained with the straws connected to the front-end electronics.

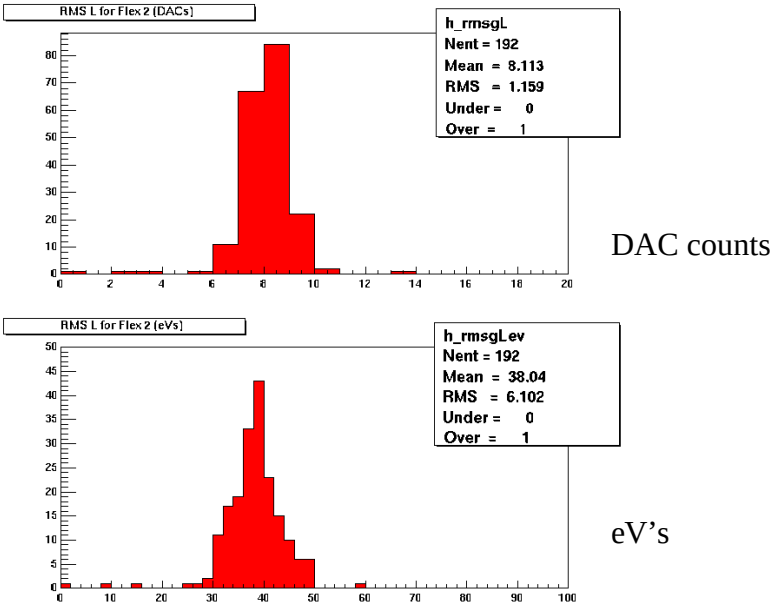

Figure 12: Sigma noise distributions for the 192 channels of the flex-rigid board in DAC counts (top) and in eV's (bottom). Results were obtained from threshold scans with the straws connected to the front-end electronics.

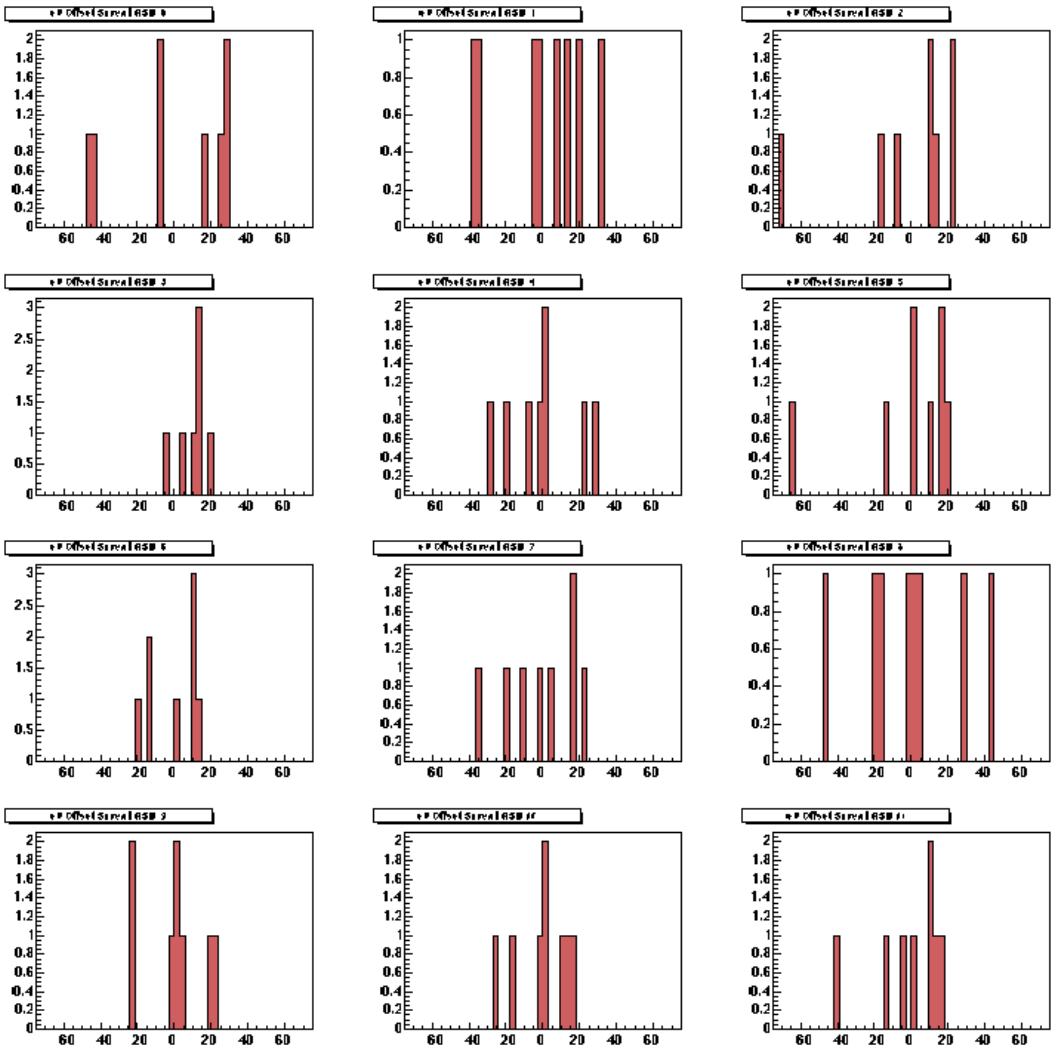

Figure 13: Offset threshold spread (in eV's) with respect to a nominal 200 eV threshold chip average for 12 of the 24 ASDBLR chips on the flex-rigid board used for the GIF irradiation

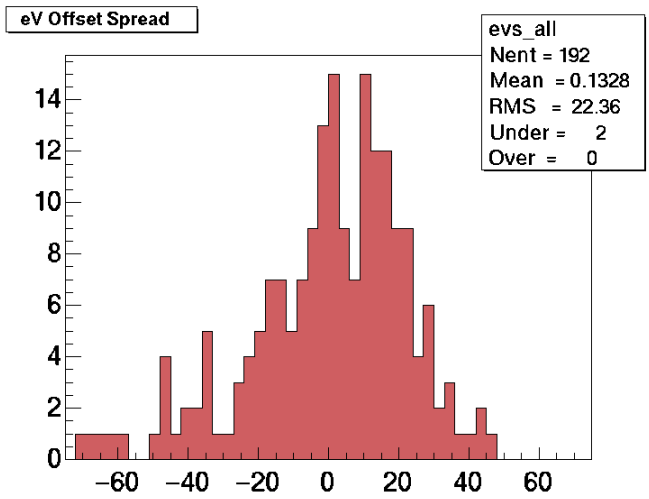

Figure 14: Offset threshold spreads (in eV's) with respect to a nominal 200 eV threshold chip average for the 192 channels of the flex-rigid board used for the GIF measurements.

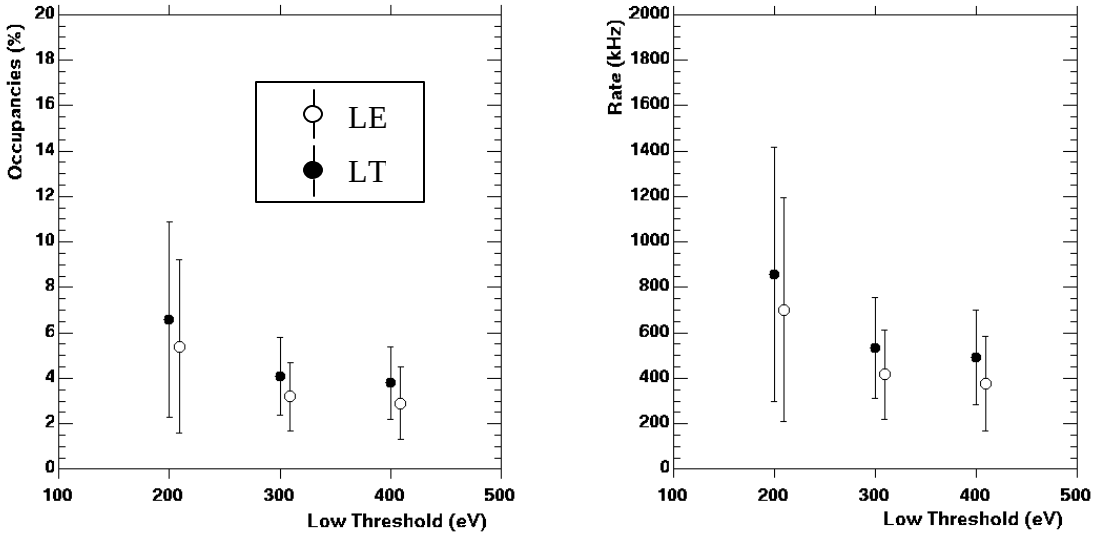

Figure 15: Low threshold (LT) and leadind edge (LE) occupancies (in %) and noise rates (in k Hz) as a function of low threshold (in eV's) under GIF irradiation. Occupancies and rates are averaged over 192 channels of the flex-rigid board and are calculated for 3 beam crossings.

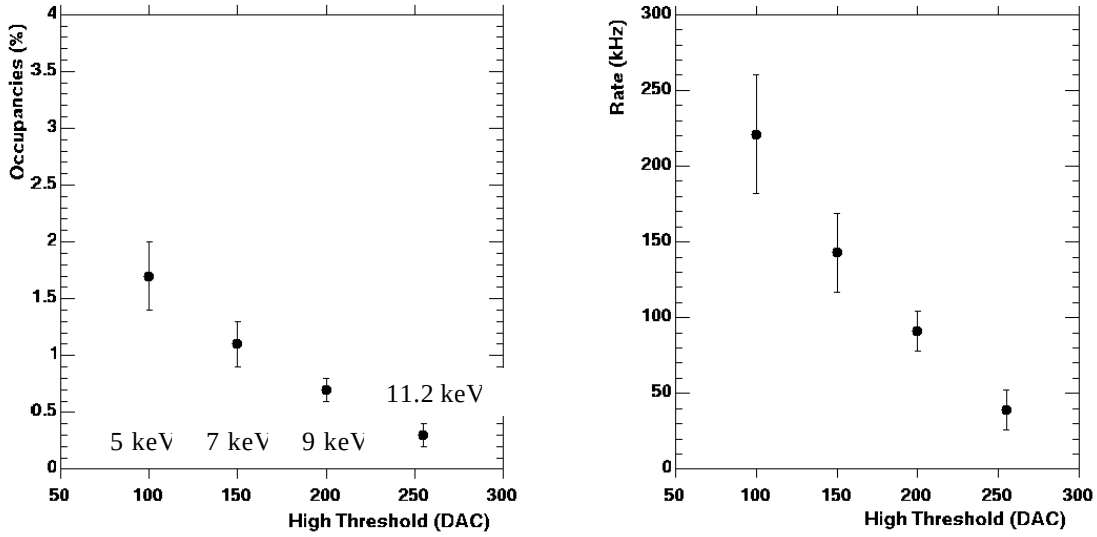

Figure 16: High threshold occupancies (in %) and noise rates (in kHz) as a function of high threshold (in DAC counts and keV's) under GIF irradiation. Occupancies and rates are averaged over 192 channels of the flex-rigid board and are calculated for 3 beam crossings.

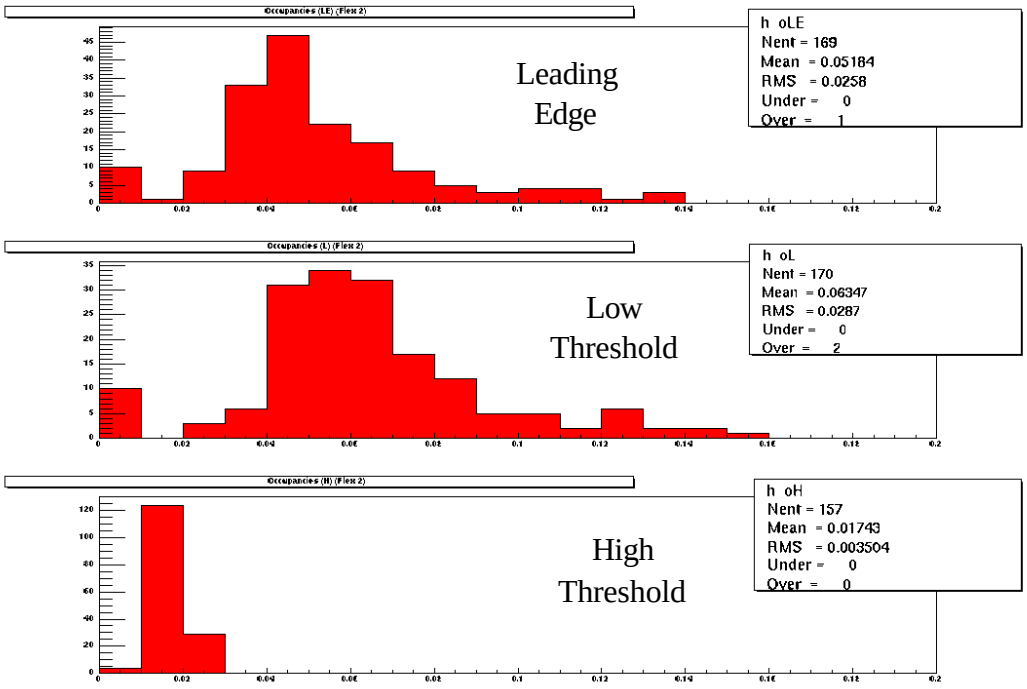

Figure 17: Distribution of leading edge hit occupancies (top), low threshold hit occupancies (middle), and high threshold hit occupancies (bottom) for the 192 channels of the flex-rigid board under GIF irradiation. A low threshold of 200 eV and a high threshold of 5 keV were used.

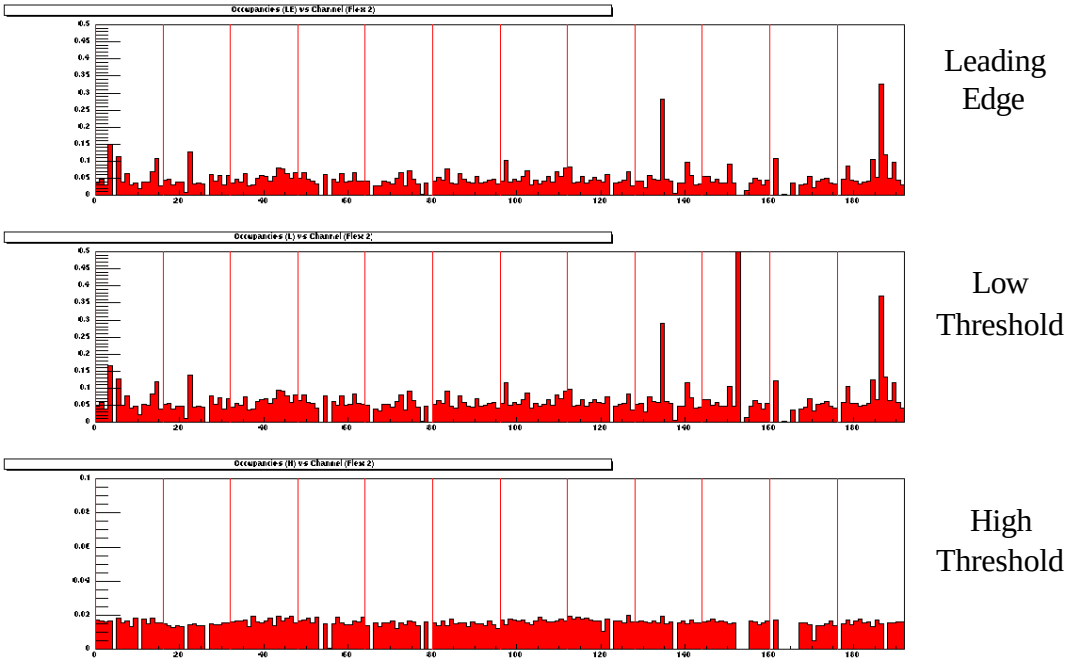

Figure 18: Leading edge (top), low threshold (middle), and high threshold (bottom) occupancy distributions as a function of channel number under GIF irradiation. A nominal low threshold of 200 eV and a high threshold of 5 keV were used.

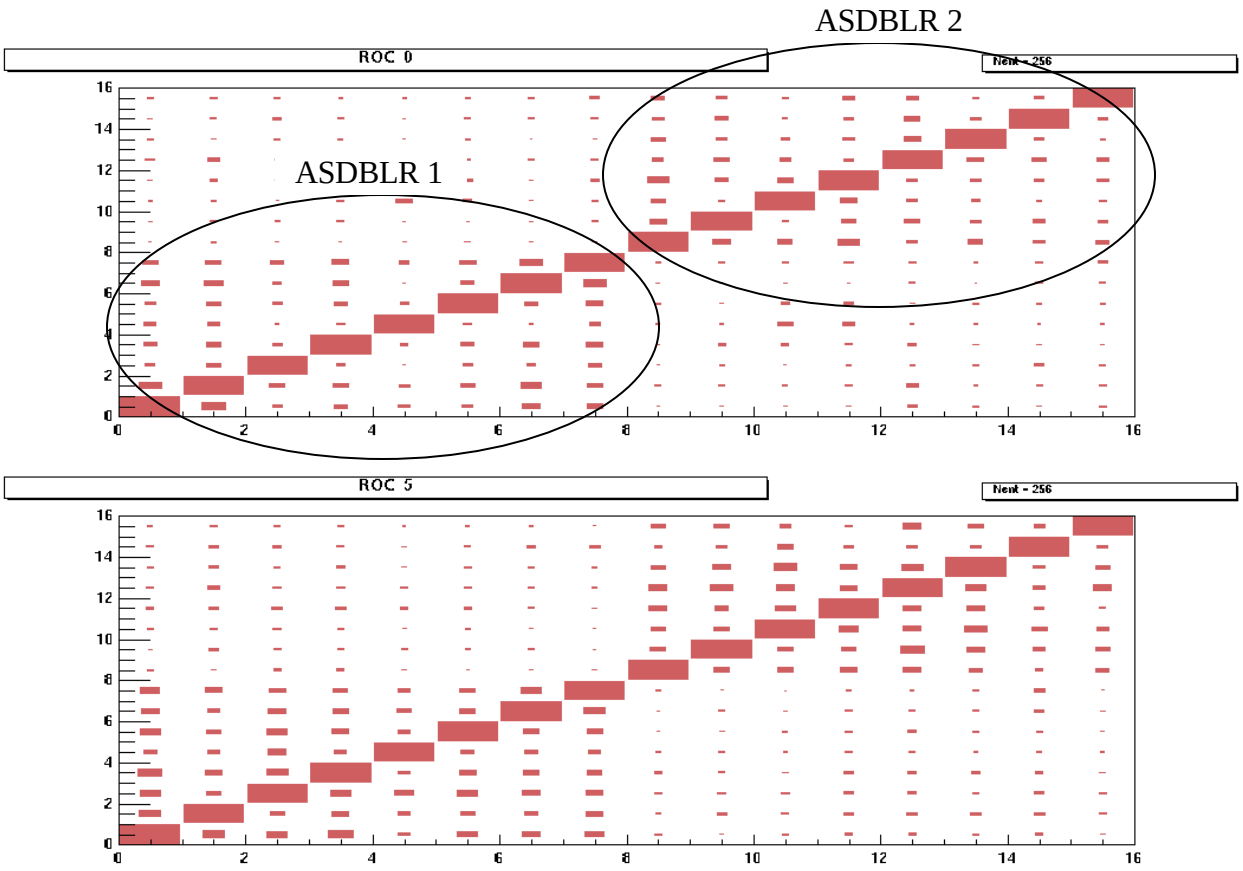

Figure 19: Occupancy correlation matrix for two different DTMROC chips (DTMROC 0 on top and DTMROC 5 on bottom) of the flex-rigid board under GIF irradiation. Each DTMROC chip contains 2 ASDBLR HV groups (ASDBLR1 and ASDBLR2) where cross-talk is visible.

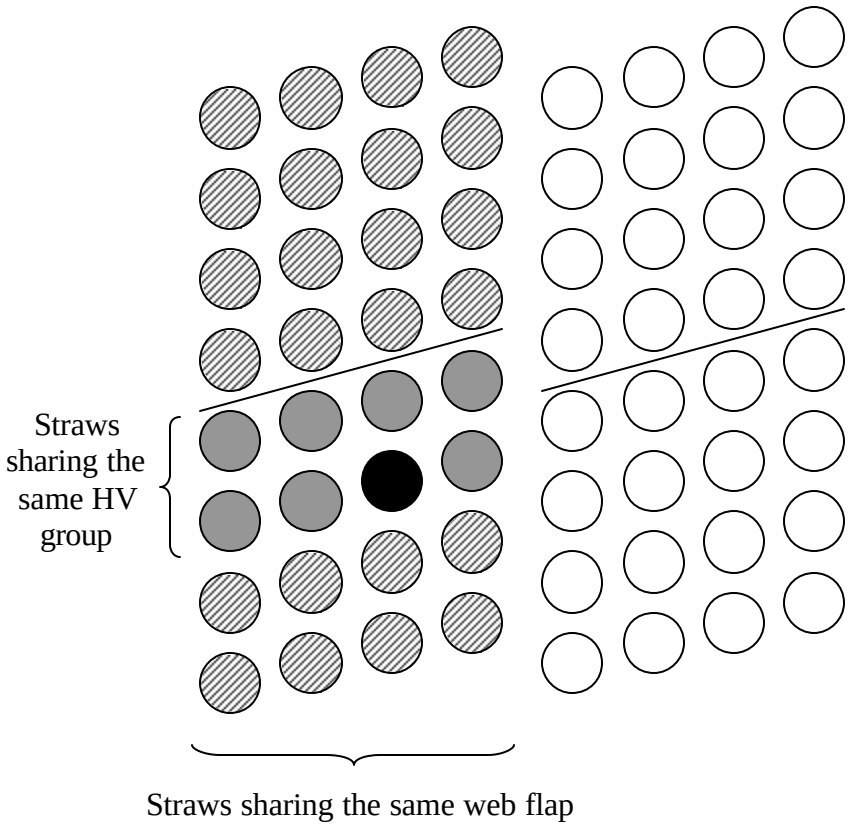

Figure 20: Diagram of 4 DTMROC chips of the sector prototype with the placement of the trigger straw (on black), the straws sharing the same HV group as the *trigger straw* (7 straws on grey), 24 straws sharing the same web flap as the *trigger straw* (dashed), and part of the 32 away straws placed on different web flaps as the *trigger straw* (white).

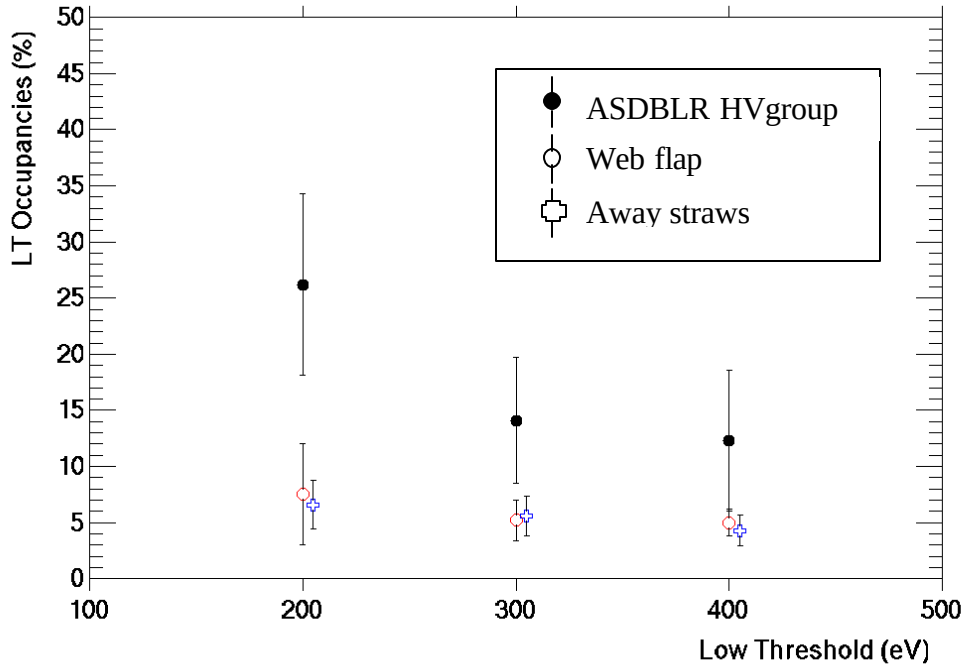

Figure 21: Average low threshold occupancies (in %) as a function of low threshold (in eV's) under GIF irradiation for the 3 sets of straws defined in Section 5.1. All values are calculated for events with a high threshold hit above 5 keV on the *trigger straw*.

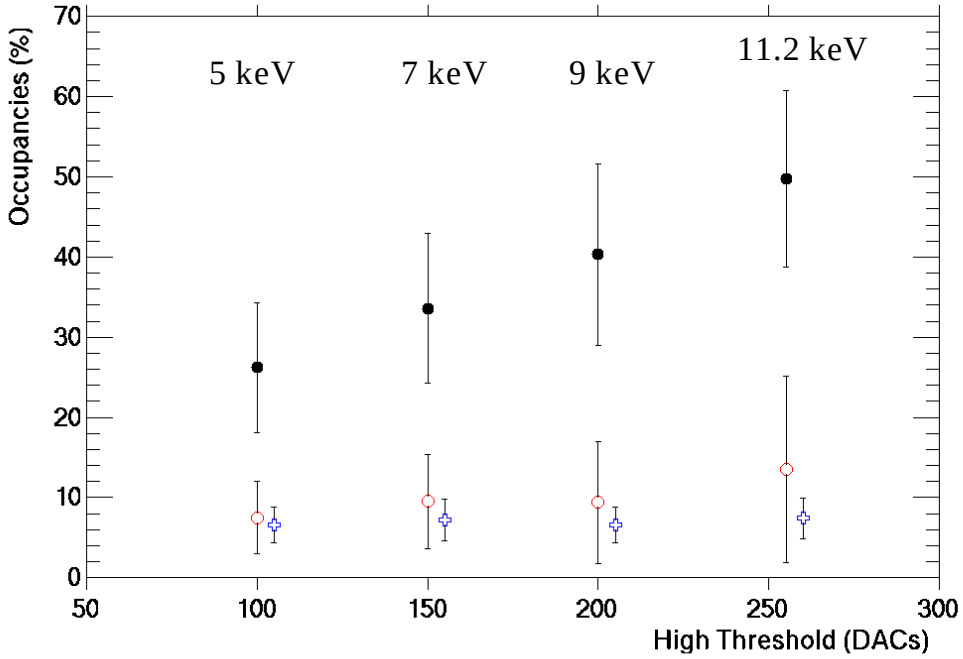

Figure 22: Average low threshold occupancies (in %) for the 3 sets of straws defined in Section x as a function of the high threshold set on the *trigger straw*. All values are calculated for a 200 eV low threshold.

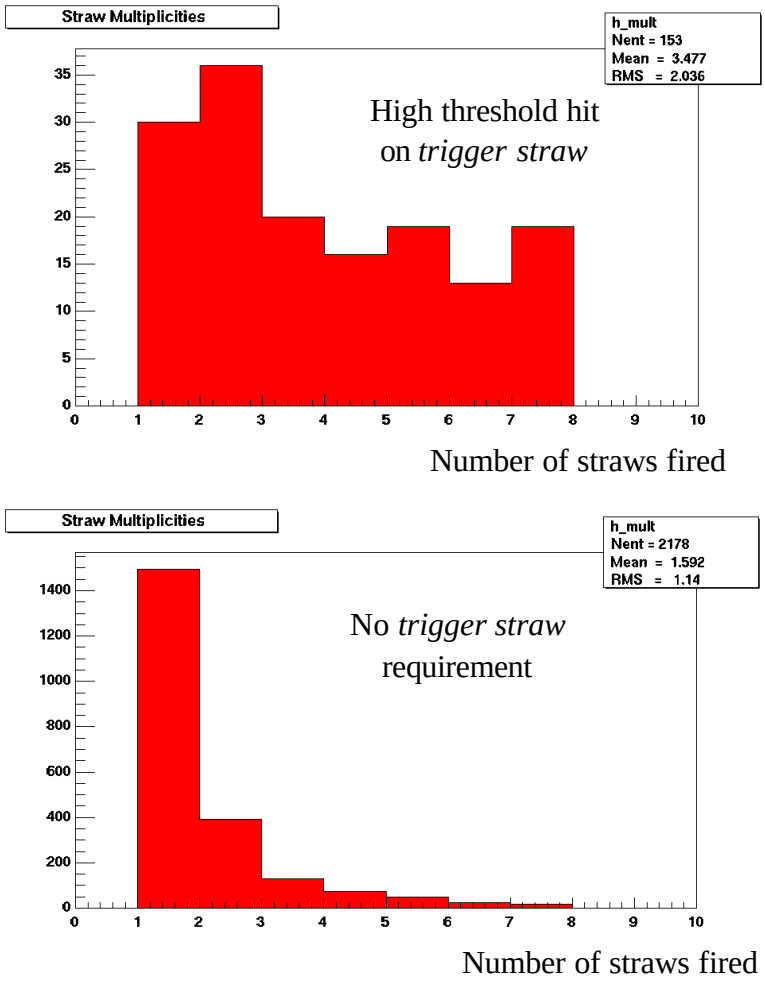

Figure 23: Straw hit multiplicity distribution for those straws sharing the same HV group as the *trigger straw* when a high threshold hit above 5 keV is required on the *trigger straw* (top) and when no high threshold hit is required on the *trigger straw* (bottom).

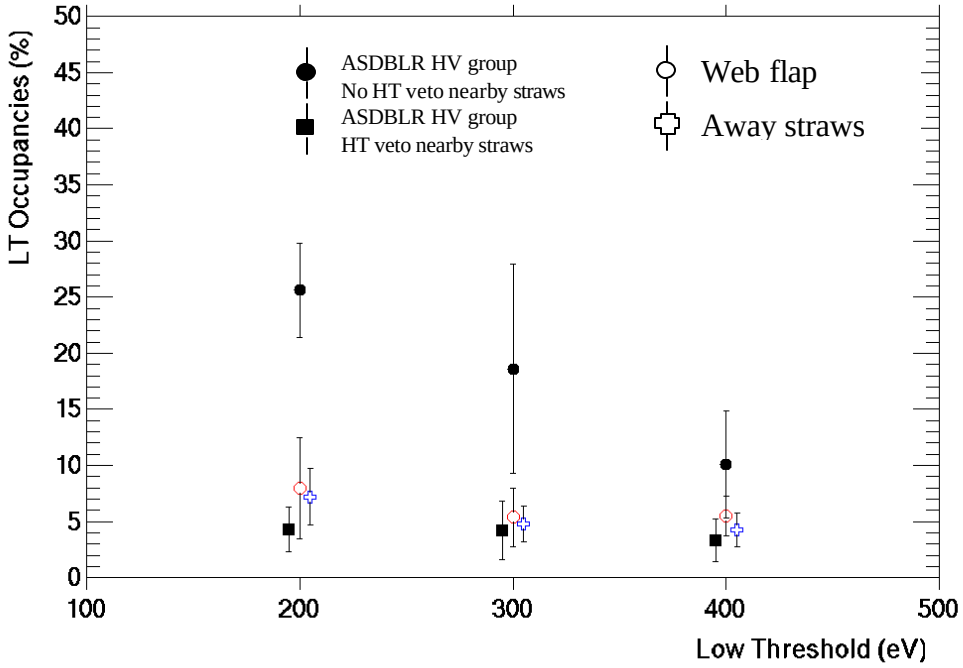

Figure 24: Average low threshold occupancies (in %) as a function of low threshold (in eV's) for the 3 sets of straws defined in Section x. All values are calculated for events with a leading edge hit on the *trigger straw*. The occupancies for the straws sharing the same HV group as the *trigger straw* are also shown when a high threshold veto is required on the nearby straws to the *trigger straw*.

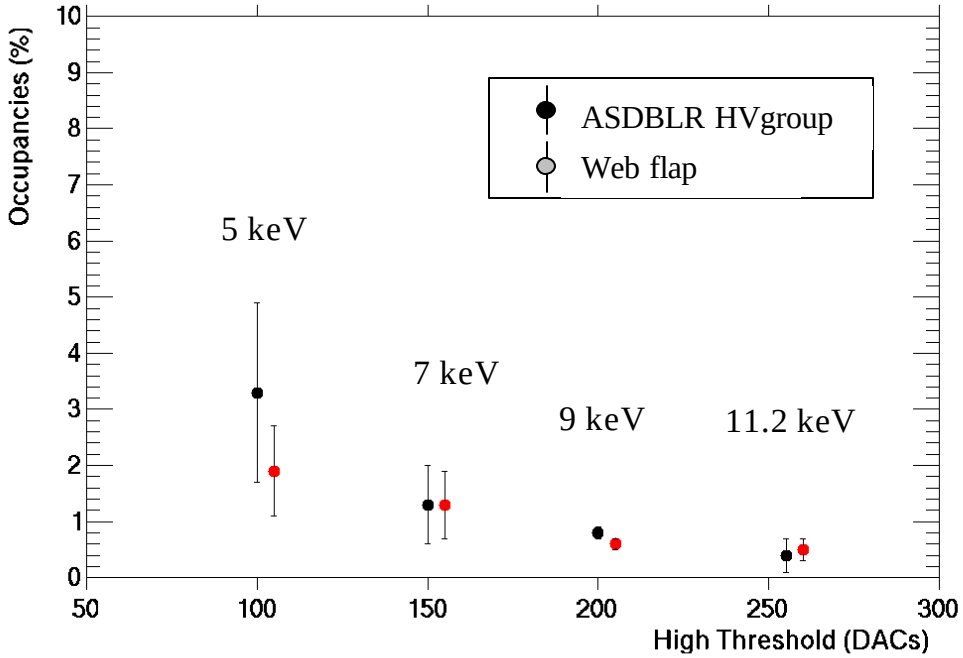

Figure25: Average high threshol d occupancies (in %) as a function of the high threshold (in DAC counts and keV's) of the *trigger straw*.